Outer membrane vesicles produced by pathogenic strains of *Escherichia coli* block autophagic flux and exacerbate inflammasome activation

Laure David[a#], Frédéric Taieb[a#], Marie Pénary[a], Pierre-Jean Bordignon[b], Rémi Planès[b], Valérie Duplan-Eche[c], Etienne Meunier[b], Eric Oswald[a,d*]

[a]IRSD, INSERM, ENVT, INRAE, Université de Toulouse, UPS, Toulouse, France ; [b]Institute of Pharmacology and Structural Biology (IPBS), University of Toulouse, 9 CNRS, Toulouse, France ; [c]INFINITy, Université de Toulouse, CNRS, INSERM, UPS, Toulouse, France ; [d]CHU Toulouse, Hôpital Purpan, Service de Bactériologie-Hygiène, Toulouse, France.

# These authors contributed equally

*Address correspondence to: eric.oswald@inserm.fr

Outer membrane vesicles produced by pathogenic strains of *Escherichia coli* block autophagic flux and exacerbate inflammasome activation

Escherichia coli (E. coli) strains are responsible for a majority of human extra-intestinal infections, resulting in huge medical, economic and social costs. We had previously shown that HlyF encoded by a large virulence plasmid harbored by pathogenic *E. coli* is not a hemolysin but a cytoplasmic enzyme leading to the overproduction of outer membrane vesicles (OMVs). Here, we show that these specific OMVs inhibit the autophagic flux by impairing the autophagosome – lysosome fusion, thus preventing the formation of acidic autolysosome and autophagosome clearance. Furthermore, OMVs from *E. coli* producing HlyF are much more prone to activate the non-canonical inflammasome pathway. Since autophagy and inflammation are crucial in the host's response to infection especially during sepsis, our findings reveal an unsuspected role of OMVs in the crosstalk between bacteria and their host, highlighting the fact that these extracellular vesicles have exacerbated pathogenic properties compared to OMVs produced by isogenic strains unable to produce a functional HlyF.

Keywords: Outer Membrane Vesicle; *Escherichia coli*; HlyF; pathogenesis; autophagy; inflammasome

Abbreviations:

AIEC: adherent-invasive *E. coli*
BDI: Bright Detail Intensity
BMDM: bone marrow-derived macrophages
Casp: Caspase
E. coli: *Escherichia coli*
EHEC: enterohemorrhagic *E. coli*
ExPEC*:* extra-intestinal pathogenic *E. coli*
GSDM-D: Gasdermin-D
GFP: Green Fluorescent Protein
HBSS: Hanks'balanced salt solution
HlyF: Hemolysin F
IL-1β : interleukin-1β
ISX: ImageStreamX system
LPS: Lipopolysaccharide
OMV: outer membrane vesicle
RFP: Red Fluorescent Protein
TEM: transmission electron microscopy
WT: Wild type
Mut: Mutated

Introduction

Although the majority of *E. coli* strains are commensal bacteria colonizing the digestive tract, some are pathogenic because they have acquired an arsenal of virulence factors that allow them to overcome innate or acquired defense mechanisms of their host (Sarowska et al., 2019). HlyF is a bacterial protein encoded by a gene present on a virulence plasmid found in strains of *E. coli* responsible for extraintestinal infection in both human and animal (Peigne et al., 2009). More specifically, it is found in strains responsible for neonatal meningitis, avian colibacillosis (Johnson et al., 2008; Kim et al., 2020; de Oliveira et al., 2015) and more recently in an emerging serovar of enterohemorrhagic *E. coli* (EHEC) responsible for hemolytic and uremic syndrome in human (Soysal et al., 2016). *HlyF* does not code for hemolysin as its name would suggest, but for a cytoplasmic protein that contributes to the bacterial virulence (Murase et al., 2016). The HlyF protein displays a predicted catalytic domain of the short-chain dehydrogenase/reductase superfamily. This conserved domain is involved the ability of HlyF to promote the production of bacterial OMVs (Murase et al., 2016). OMVs are nanoparticles consisting of a lipid bilayer including membranous proteins and LPS originating from the parental strain and containing luminal cargos (Jan, 2017; Schwechheimer and Kuehn, 2015). Similarly to eukaryotic exosomes and microvesicles, OMVs are a mean of communication between bacteria and eukaryotic host cells (Kuehn and Kesty, 2005; Kulp and Kuehn, 2010). Interestingly, we have observed that culture supernatants of *E. coli* strains expressing HlyF induced autophagic vacuoles in host cells (Murase et al., 2016). At that time, we thought we were observing an exacerbation of autophagy and we interpreted this phenotype as related to the greater quantity of OMVs present in the supernatant.

Here, we show that extracellular vesicles from *E. coli* strains producing HlyF have exacerbated pathogenic properties compared to OMVs produced by isogenic strains unable to produce a functional HlyF. Our results revealed that these OMVs inhibit the autophagic flux and are much more prone to overactivate the non-canonical inflammasome pathway, the main host defense mechanism against infections that must be tightly regulated to ensure a correct antimicrobial response. Autophagy is one of the main negative regulator of inflammasome activation and plays a protective role in inflammatory diseases such as sepsis (Biasizzo and Kopitar-Jerala, 2020; Feng et al., 2019; Ho et al., 2016; Qiu et al., 2019). Thus, these OMVs, produced by bacteria responsible of extraintestinal infections, could destabilize the host response to the infection, thus facilitating its progression.

Results

OMVs from HlyF-expressing Escherichia coli specifically induce an increase of autophagosomes numbers

In agreement with our previous results (Murase et al., 2016), bacterial expression of wild type (WT) HlyF is associated with an overproduction of OMVs (**Fig. 1A**). Moreover, HeLa cells treatment with culture supernatant of these HlyF WT strains induces an increase of autophagosomes number in host cells, as denoted by autophagosome-associated LC3 foci (**Fig. 1B**). Eukaryotic cells were then treated this time with the same number of purified OMVs from isogenic *E. coli* strains expressing or not HlyF. To do so, we analyzed OMVs by TEM and checked that the concentration of OMVs is correlated to protein concentration (data not shown). Consistent with our previous results, at the same concentration, only OMVs from the wild type strain expressing HlyF specifically induce an increase of autophagosomes number in host cells (**Fig. 1C**). A dose effect shows that no matter how much OMVs of the non-HlyF producing strain are put on the

HeLa cells, no autophagosome accumulation is ever observed (data not shown). We repeated these experiments using the same amount of OMVs purified from the laboratory *E. coli* strain BL21 (DE3) devoid of virulence factors and flagellin, expressing wild-type or inactivated HlyF (**Suppl. Fig 1A**). OMVs were analyzed by TEM (**Fig. 1D**), but also by dynamic light scattering (**Suppl. Fig. 1B**) and we performed protein and LPS dosages (**Suppl. Fig. 1C**) to refine their characterization. These results showed that OMVs produced from both strains expressing active and inactive HlyF have a similar diameter (25.95nm +/- 4.91 and 24.5nm +/- 4.86 respectively) and comparable concentration of protein and LPS per vesicle. The increase of LC3-GFP-associated autophagosomes (**Fig. 1E**) as well as the increase of LC3-II level (**Fig. 1F**) in OMVs intoxicated cells confirmed the specific HlyF-dependent alteration of autophagy following cell treatment with OMVs from BL21-producing wild type HlyF.

Increased autophagosomes numbers induced by OMVs from HlyF-expressing E. coli is dose-dependent and persistent

To quantify the number of autophagosomes per cell, we counted the fluorescently labelled GFP-LC3 puncta per cell using the imaging flow cytometry technology (ImageStreamX system – ISX) (Pugsley, 2017). The quantification of dots of GFP-LC3 per cell shows that OMVs HlyF WT treatment induces a 5-fold increase of autophagosomes in eukaryotic cells compared to non-treated cells (**Fig. 2A –B).** To evaluate the kinetic of OMV-induced increase of autophagosomes in the host cell, we performed time-course experiments. Measurement of the level of LC3-II at different time points in HeLa cells showed that autophagosome increase in HeLa cells lasted at least 72 hours after the beginning of OMV HlyF WT treatment (**Fig. 2C**). Finally, we also showed that the

accumulation of autophagosomes increases with the concentration of OMVs HlyF WT until it reaches a plateau from a concentration of 4µg/mL of OMVs (**Fig. 2D**).

OMVs from HlyF-expressing E. coli induce an autophagic blockade

Autophagy is a dynamic process in which the number of autophagosomes depends on their formation and further degradation. This is referred as autophagic flux. Thus, OMV-dependent accumulation of autophagosomes could result either from an increased synthesis of autophagosomes or from a decreased degradation following their fusion with lysosome (**Fig. 3A**) (Mizushima et al., 2010; Muñoz-Braceras and Escalante, 2016). To decipher the cellular basis of increase of autophagosomes number after OMV treatment, we monitored the level of autophagosomes-associated LC3-II in HeLa cells. As expected, LC3-II level increased when lysosomal-dependent LC3-II degradation is blocked by the lysosomal inhibitor chloroquine. However, these levels were comparable in cells treated with OMVs in presence of chloroquine (**Fig. 3B, lines 2 and 4**). Absence of cumulative effect of OMVs and chloroquine on LC3-II level suggests that OMVs HlyF WT induce an autophagy blockade in HeLa cells similarly to chloroquine treatment. These results were confirmed by quantification of GFP-LC3 cells treated by OMVs HlyF WT in presence or absence of chloroquine by imaging flow cytometry. We observed that the number of GFP-LC3 fluorescent dots in OMV-treated cells is not further increased by chloroquine (**Fig. 3C-D**). Altogether, these results showed that OMVs HlyF WT treatment induces an autophagic blockade in eukaryotic cells rather than an induction of the flux.

OMVs from HlyF-expressing Escherichia coli prevents the formation of acidic compartments and autophagosomes clearance.

We then investigated which step of the autophagy pathway was inhibited. We first observed that OMVs were not sequestered inside the autophagosomes, as there is no co-localisation between GFP-LC3 structures and OMV stained with DiI (**Suppl. Fig 2**). We then used the HeLa-Difluo hLC3 cell line. These cells express a fusion protein RFP::GFP::LC3, in which the N-terminus of LC3 is fused to two fluorescent reporter proteins: a RFP (acid-stable) and a GFP (acid-sensitive). Autophagosomes that contain intact RFP::GFP::LC3 proteins emit both RFP and GFP signals resulting in a yellow fluorescence. After fusion of the autophagosomes with the lysosomes, the GFP fluorescence diminishes due to the acidification of the autophagolysosome, while a red fluorescence corresponding to the remaining acidic -resistant RFP-LC3 signal is maintained (Kimura et al., 2007; Loos et al., 2014). We performed confocal imaging of HeLa-Difluo hLC3 cells. As expected, in the control condition treated with lysosomal inhibitor chloroquine, we observed an accumulation of yellow punctae corresponding to autophagosomes harboring GFP and RFP LC3. When cells were starved with HBSS, known to induce the autophagic flux, a proportion of GFP fluorescence was decreased by the acidic pH environment while acid-resistant red fluorescence persisted, denoting that fusion of autophagosome with lysosome occured in these cells. In contrast, in cells treated with OMVs HlyF WT, we observed an increased number of yellow punctae (resulting from both autophagosome-associated GFP and RFP fluorescence) indicating that the autophagic blockade occurs before the acidification of the autophagosomal compartments (**Fig. 4A**).

To confirm this result, we quantified the level of fluorescently labelled RFP and GFP LC3 in HeLa-Difluo hLC3 by imaging flow cytometry. In contrast to starvation but similarly to chloroquine treatment, we observed that in cells treated by OMVs the ratio

RFP/GFP in low, indicating that the GFP is preserved from autophagosome acidification (**Fig 4B-C**).

Finally, we stained acidic organelles in GFP-LC3 cells with LysoTracker Red labelling. We checked that upon starvation, GFP-LC3 Hela cells harbored yellow structures (highlighted by white arrows) resulting from the co-localization of autophagosomes and lysosomes merged signals. In contrast, absence of yellow punctae indicated that OMVs HlyF WT treatment of GFP-LC3 HeLa cells prevented lysosomal acidification of autophagosomes (**Fig. 4D**). These results showed that autophagy flux is blocked by OMV at lysosomal fusion step.

OMVs from HlyF-expressing E. coli induce a stronger activation of the non-canonical inflammasome pathway compared to OMVs from E. coli expressing a non-functional HlyF protein.

Numerous studies showed that autophagy is a negative regulator that prevents excessive activation of inflammasomes (Biasizzo and Kopitar-Jerala, 2020; Deretic et al., 2013; Harris et al., 2017; Krakauer, 2019; Netea-Maier et al., 2015; Qian et al., 2017). We therefore speculated that OMV-dependent inhibition of autophagic flux could exacerbate inflammasome activation. OMV-treatment of mice bone marrow-derived macrophages (BMDM) leads to the excretion of IL-1β in the supernatant of cell culture. This phenotype is dependent of the activation of the non-canonical inflammasome pathway since it is abolished in inflammasome-deficient BMDM (Caspase (Casp)-11$^{-/-}$ and Casp-1$^{-/-}$/Casp-11$^{-/-}$ BMDM). Furthermore, IL-1ß secretion is exacerbated when BMDM were treated with OMVs HlyF WT compared to OMVs produced in bacteria expressing inactive HlyF (**Fig. 5A**). Since activation of the non-canonical inflammasome pathway is related to the sensing of LPS through host guanylate-binding proteins in the cytosol (Santos et al.,

2018), we transfected purified LPS from OMVs HlyF WT and from OMVs HlyF Mut directly into the cytosol of BMDM. Interestingly, we found that the activation of the non-canonical inflammasome pathway, measured by Caspase-1 (Casp-1) and Gasdermin-D (GSDM-D) cleavage and release in the supernatant, was similar regardless of the LPS transfected (**Fig. 5B, lines 7 and 9**). This result suggests that the overactivation of the non-canonical inflammasome pathway does not depend on LPS difference but rather results from OMV HlyF WT ability to block the autophagy.

Discussion

In this study we confirmed previous results published by (Murase et al., 2016) namely that pathogenic *E. coli* harboring a virulence plasmid encoding *hlyF* gene overproduce OMVs that modulate autophagy. But here we showed that this modulation was due to an autophagic blockage instead of an induction of the flux as initially thought. Moreover, we uncovered the mechanistic explanation of this result and demonstrated that OMVs HlyF WT block autophagosome maturation and fusion with lysosomes. Autophagy is recognized as an innate antibacterial mechanism by direct lysosomal degradation of intracellular pathogen. After engulfment of the cytosolic pathogen, autophagosomes fuse with lysosomes, leading to degradation of the sequestered content (Netea-Maier et al., 2015). Thus, autophagic and lysosomal degradation pathways that are crucial to maintain cellular homeostasis, act also as the first line of host defense against bacterial pathogen as it fights against the intruder very early during infection (Losier et al., 2019). It has been shown recently that some ExPEC hijack the autophagy machinery to promote their intracellular survival and replication in macrophages. This ability is due to the expression of HlyF that prevents the fusion of ExPEC-containing phagosomes with lysosomes and their subsequent degradation (Zhuge et al., 2018). This

property could be due to production of OMVs with the properties we demonstrated here, preventing phagolysosomal fusion and acidification in macrophages. In line with this idea, the fact that the adherent-invasive *E. coli* (AIEC) reference strain NRG 857Cc harbors the *hlyF* gene suggests that OMVs actively participate in the virulence of these pathogenic bacteria by favoring the invasion, the survival and their replication into macrophages (McPhee et al., 2014). OMVs is also known to facilitate the internalization of AIEC into intestinal cells (Rolhion et al., 2005). These results together with those deciphered here highlight that pathogenic bacteria could exploit HlyF OMV property to block their autophagosomal clearance into epithelial cells and macrophages.

Thus, the contribution of HlyF and OMVs to bacterial virulence includes autophagic blockage but also the dissemination and delivery of their virulence factors sometimes far from the source of infection, directly into the cytoplasm of target cells. In line with this idea, OMVs play a very important role in mediating the cytosolic localization of lipopolysaccharide (LPS), an endotoxin that is present at their surface. Once in the host cytosol, LPS is recognized by the non-canonical inflammasome machinery and thereby activates an inflammatory immune response (Kaparakis-Liaskos and Ferrero, 2015; Santos et al., 2018; Vanaja et al., 2016). However, excessive inflammation activation by LPS can be deleterious for the host, mainly through inflammasome activation and dysregulated cell death induction that will trigger an exacerbated and pathological host immune response. In particular, OMVs produced by AIEC play a role in the physiopathology of chronic inflammatory diseases such as Crohn's disease (Rolhion et al., 2005). The inflammatory burst they cause can also lead to organ dysfunction which can worsen up to sepsis in severe cases (Chen et al., 2018; Schroder et al., 2018). At the early stage of sepsis, macrophages release large amounts of

pro-inflammatory molecules that exacerbate inflammatory response. It is then followed by an immunosuppression due to the excessive apoptosis of macrophages, which makes host susceptible to recurrent infections (Cecconi et al., 2018; van der Poll et al., 2017). The role of OMVs in sepsis is highlighted by the fact that injection of OMVs alone in mice recapitulates sepsis-associated exacerbated inflammation and mortality (Eren et al., 2020). Thus, this inflammation machinery initiated by OMV recognition must be tightly regulated. Here we show that OMV HlyF WT provoke an exacerbated activation of the non-canonical inflammasome activation and IL-1β release, one of the main mechanisms through which innate and adaptive immune responses are induced by an infection (Eren et al., 2020; Gomes and Dikic, 2014; Schroder et al., 2018). We showed that not only OMVs HlyF WT induces inflammation actions via LPS presentation, they also block autophagy, a major negative regular of excessive inflammation activation and IL-1β release (Crişan et al., 2011; Saitoh et al., 2008). In particular, autophagy induction prevents the onset of sepsis (Biasizzo and Kopitar-Jerala, 2020). This negative regulation mainly relies on the removal of endogenous inflammasome agonists and through effects on the secretion of immune mediators (Deretic et al., 2013; Harris et al., 2017; Krakauer, 2019; Netea-Maier et al., 2015; Qian et al., 2017). Therefore, inhibition of autosomal clearance of inflammasome activators, such as LPS, by OMV HlyF WT impair inflammasome negative feedback control, leading to an excessive and uncontrolled inflammatory condition detrimental for the host.

This study unravels the molecular mechanisms by which HlyF expression by *E. coli* confers hyper-virulent properties to OMVs, as they gain the property to manipulate the host cell autophagic and inflammatory responses to bacterial benefit both at the site and at great distance from the site of infection. An additional contribution of OMVs HlyF

to bacterial virulence could be associated to the dissemination of toxins (notably endotoxins). Indeed, we showed that bacterial HlyF expression increases production of OMVs and that OMVs are known to carry a cocktail of toxins, such as toxin cytolysin A (ClyA), Cytolethal Distending Toxin (CDT) (Murase et al., 2016) or Shiga-toxins in OMVs from EHEC strains (Bielaszewska et al., 2017). Thus HlyF expression may also drive the massive dissemination of OMV-encapsulated toxins sometimes at great distance from the site of infection, protected from degradation, and released in their active forms to their specific cell compartments, where they can develop their detrimental effects (Rueter and Bielaszewska, 2020).

Overall, OMVs HlyF contribute significantly to the virulence of pathogenic bacteria. Further studies aiming at understanding how HlyF produces hypervirulent OMVs will be a necessary step toward development of effective strategies to fight bacterial pathogenesis.

Materials and methods

Bacterial strains and growth conditions

SP15 is an extra-intestinal pathogenic *E. coli* (ExPEC) strain isolated from a neonatal meningitis case (Johnson et al., 2002). SP15, SP15Δhlyf and SP15ΔhlyfGST-hlyF were previously described in (Murase et al., 2016). pGEX6P-1 plasmids expressing GST-HlyF protein wild type or inactivated by a mutation on its putative catalytic site (**Suppl. Fig. 1A**) were transformed *in E. coli* BL21(DE3) strain. SP15 and BL21(DE3) strains and derivatives were inoculated and grown in Terrific Broth with appropriate antibiotics for 8hr at 37°C with agitation.

Purification of bacterial OMVs

After 8hr of culture the bacterial suspension was centrifuged at 6500g for 10min at 4°C. The supernatant was filtered (pore size, 0.45µm) to obtain bacterial-free supernatant. The filtered supernatant was ultrafiltered and concentrated using tangential concentrator and PES membrane cassette (pore size, 100kDa, Sartorius) and ultracentrifuged at 150,000g for 1.5hr at 4°C. After removing the supernatant, pelleted OMV were resuspended in sterile PBS with Ca^{2+} and Mg^{2+} and stored at 4°C. To visualize the concentration of OMVs and the purity of the preparation, negative staining transmission electron microscopy (TEM) was performed according to standard procedures. Briefly, 5µL of OMV samples were added to carbon coated copper mesh grid, stained with 1% uranyl acetate for 1min and imaged with a Jeol JEM 1400 Transmission Electron Microscope. The concentration of OMVs in the suspension correlates with protein concentration evaluated by BCA protein assay (DC™ protein assay Biorad) (**Suppl. Fig. 1C**). LPS concentration in OMV was evaluated by Purpald assay as described in (Lee and Tsai, 1999). Values were normalized to glycerol concentration. OMV diameter was calculated by dynamic light scattering using Zetasizer Nano instrument (Malvern) (**Suppl. Fig. 1B**). OMVs in PBS were fluorescently labeled using 1% (v/v) DiI (Thermofisher) for 30 min at 37°C.

Purification and transfection of LPS from OMVs

LPS was extracted from purified OMV using LPS extraction kit (iNtRON biotechnology) according to manufacturer's instruction. LPS concentration was determined by Purpald assay as described in (Lee and Tsai, 1999). Transfection of cells with purified LPS was done at a concentration of 500ng/50,000 cells, using FuGeneHD (Promega) transfection reagent in Opti-MEM, as previously described (Santos et al., 2018).

Eukaryotic cell culture and treatments

HeLa cells, HeLa-LC3-GFP cells and *HeLa-Difluo* hLC3 cells (Invivogen) were cultured in DMEM with Glutamax (Sigma) supplemented with 10% fetal bovine serum (FBS). *HeLa-Difluo* hLC3 cells were maintained in growth medium supplemented with the selection antibiotic *Zeocin 200µg/mL (Invivogen).* One day before the experiment, HeLa cells were seeded at a density of 50×10^4 cells per mL in DMEM supplemented with 10% FBS. OMV treatment were done by adding directly in the medium of cell culture the volume of OMV corresponding to the amount of proteins indicated. The cells were collected 3h post-stimulation.

Bone marrow-derived macrophages (BMDM) were prepared from fresh bone marrow isolated from WT or Caspases 1/11 deficient mice. Bone marrow cells were allowed to differentiate in macrophages by incubation for 7 days in DMEM supplemented with 10% fetal calf serum (Bioconcept), 25ng/ml M-CSF (Immunotools), 10mM HEPES, and nonessential amino acids (Life Technology). One day before treatment, BMDM were seeded into 24 well plates at a density of 2.5×10^5 cells per well. OMV treatment, were done by adding the volume of OMV corresponding to the amount of proteins indicated in Opti-MEM medium. The cells and supernatant were collected 24hr post-stimulation.

Immunoblotting

Cells were stimulated with the indicated treatment or left untreated for the indicated times. Then cells were washed twice with cold PBS, lysed in NuPAGE LDS sample buffer with reducing agent (Invitrogen) and sonicated. Cell extracts were boiled for 5min at 95°C, separated by SDS-PAGE and transferred to PVDF membranes (Invitrogen). The membranes were blocked in 5% BSA in 0.1% Tween-20 in TBS and probed with primary antibodies. The primary antibodies used were Rabbit anti-LC3 (Cell Signaling S 3868), Mouse anti-actin (Abcam Ab 3280), Mouse anti-Caspase-1 (Addipogen AG20B-0042), Rabbit anti-Gasdermin D (Abcam ab209845), Rabbit anti-GAPDH (GeneTex

GTX100118). After incubation with Goat anti-Rabbit and Goat anti-Mouse HRP-conjugated secondary antibodies (Promega), proteins were visualized using chemiluminescent peroxidase substrat (ECL) detection reagents (Sigma), and acquired by the ChemiDoc XRS+ System (BioRad).

Fluorescence microscopy

GFP-LC3 HeLa cells or *HeLa-Difluo* hLC3 cells were seeded onto Nunc Lab-Tek Chamber Slide system 8 wells (Sigma). The day of the experiment, cells were stimulated with the indicated treatment or left untreated for the indicated times. LysoTracker Red (Invitrogen) staining was achieved by adding the Lysotracker probe at a final concentration of 50nM directly in the medium of cell culture for 1hr. Then the cells were washed and fixed with 4% paraformaldehyde for 15min on ice. DNA was visualized using Fluoroshield with 4,6-diamidino-2-phenylindole (DAPI, Sigma). Images were acquired using a Zeiss LSM 710 confocal microscope and subsequently processed using the ImageJ software package.

Measurement of IL-1β release

Quantification of IL-1β secretion in cell supernatant was measured by ELISA (Invitrogen, IL-1 beta Mouse Uncoated ELISA Kit, # 88-7013-88), according to the manufacturer's instructions.

Imaging Flow Cytometry

GFP-LC3 HeLa cells or HeLa Difluo hLC3 cells were stimulated with the indicated treatment or left untreated for the indicated times. Then the cells were washed, trypsinized, fixed with 4% paraformaldehyde for 15min on ice. Image of each cell was acquired while they were run on the **ImageStreamX Mark II (Amnis-EMD Millipore)** at 5×10^7 cells per mL in PBS. In each experiment 5,000 (GFP+) events per sample were acquired (ensuring a sufficient number of events remaining for statistically robust

analysis) at 60X magnification. Single stain samples were also collected using the same settings and used as compensation controls to generate compensation matrice.

Image analysis was completed using image-based algorithms in the ImageStream Data Exploration and Analysis Software (IDEAS_6.2.64.0, EMD Millipore). The number of GFP-LC3 puncta per cell was assessed with the feature "Spot Counting". A mask based on GFP-LC3 staining was employed (SpotCount (M02, LC3, Bright, 16, 2, 1)) to visualize the GFP-LC3 puncta. A feature in the IDEAS software called Bright Detail Intensity R7 (BDI) was used to assess the intensity of bright spots in the cell image that have radii smaller than a threshold size (7 pixels in this study), while neglecting background staining. The ratio of BDI RFP/ BDI GFP brightness was thus assessed. The same masks and features were automatically applied for each condition.

Acknowledgments: We gratefully acknowledge the imaging platform of INFINITy institute. We also thank the transmission electronic microscopy integrative platform (METi, Toulouse) and specially Vanessa Soldan for technical help, Emmanuel Ravet (Invivogen, Toulouse) for providing us *HeLa-Difluo* hLC3 cells and Marie-Charline Blatche (LAAS institute, Toulouse) for assistance in DLS analysis. Finally, we are indebted to Dr MS, Dr J-PM and Dr J-PN for their insightful comments on the manuscript.

Fundings: This project was funded by ERC StG grant (INFLAME 804249) to EM and RP.

Disclosure of interest: The authors declare that they have no conflict of interest.

Supplementary materials

Suppl. figure S1
Suppl. figure S2

References

Biasizzo, M., and Kopitar-Jerala, N. (2020). Interplay Between NLRP3 Inflammasome and Autophagy. Front. Immunol. *11*.

Bielaszewska, M., Rüter, C., Bauwens, A., Greune, L., Jarosch, K.-A., Steil, D., Zhang, W., He, X., Lloubes, R., Fruth, A., et al. (2017). Host cell interactions of outer membrane vesicle-associated virulence factors of enterohemorrhagic Escherichia coli O157: Intracellular delivery, trafficking and mechanisms of cell injury. PLOS Pathog. *13*, e1006159.

Cecconi, M., Evans, L., Levy, M., and Rhodes, A. (2018). Sepsis and septic shock. Lancet Lond. Engl. *392*, 75–87.

Chen, K.W., Monteleone, M., Boucher, D., Sollberger, G., Ramnath, D., Condon, N.D., von Pein, J.B., Broz, P., Sweet, M.J., and Schroder, K. (2018). Noncanonical inflammasome signaling elicits gasdermin D-dependent neutrophil extracellular traps. Sci. Immunol. *3*.

Crişan, T.O., Plantinga, T.S., van de Veerdonk, F.L., Farcaş, M.F., Stoffels, M., Kullberg, B.-J., van der Meer, J.W.M., Joosten, L.A.B., and Netea, M.G. (2011). Inflammasome-independent modulation of cytokine response by autophagy in human cells. PloS One *6*, e18666.

Deretic, V., Saitoh, T., and Akira, S. (2013). Autophagy in infection, inflammation and immunity. Nat. Rev. Immunol. *13*, 722–737.

Eren, E., Planès, R., Bagayoko, S., Bordignon, P.-J., Chaoui, K., Hessel, A., Santoni, K., Pinilla, M., Burlet-Schiltz, O., Howard, J.C., et al. (2020). Irgm2 and Gate-16 cooperatively dampen targeting of caspase-11 to Gram-negative bacterial products. BioRxiv 2020.03.06.980433.

Feng, Y., Liu, B., Zheng, X., Chen, L., Chen, W., and Fang, Z. (2019). The protective role of autophagy in sepsis. Microb. Pathog. *131*, 106–111.

Gomes, L.C., and Dikic, I. (2014). Autophagy in antimicrobial immunity. Mol. Cell *54*, 224–233.

Harris, J., Lang, T., Thomas, J.P.W., Sukkar, M.B., Nabar, N.R., and Kehrl, J.H. (2017). Autophagy and inflammasomes. Mol. Immunol. *86*, 10–15.

Ho, J., Yu, J., Wong, S.H., Zhang, L., Liu, X., Wong, W.T., Leung, C.C.H., Choi, G., Wang, M.H.T., Gin, T., et al. (2016). Autophagy in sepsis: Degradation into exhaustion? Autophagy *12*, 1073–1082.

Jan, A.T. (2017). Outer Membrane Vesicles (OMVs) of Gram-negative Bacteria: A Perspective Update. Front. Microbiol. *8*.

Johnson, J.R., Oswald, E., O'Bryan, T.T., Kuskowski, M.A., and Spanjaard, L. (2002). Phylogenetic distribution of virulence-associated genes among Escherichia coli isolates associated with neonatal bacterial meningitis in the Netherlands. J. Infect. Dis. *185*, 774–784.

Johnson, T.J., Wannemuehler, Y., Doetkott, C., Johnson, S.J., Rosenberger, S.C., and Nolan, L.K. (2008). Identification of minimal predictors of avian pathogenic Escherichia coli virulence for use as a rapid diagnostic tool. J. Clin. Microbiol. *46*, 3987–3996.

Kaparakis-Liaskos, M., and Ferrero, R.L. (2015). Immune modulation by bacterial outer membrane vesicles. Nat. Rev. Immunol. *15*, 375–387.

Kim, Y.B., Yoon, M.Y., Ha, J.S., Seo, K.W., Noh, E.B., Son, S.H., and Lee, Y.J. (2020). Molecular characterization of avian pathogenic Escherichia coli from broiler chickens with colibacillosis. Poult. Sci. *99*, 1088–1095.

Kimura, S., Noda, T., and Yoshimori, T. (2007). Dissection of the autophagosome maturation process by a novel reporter protein, tandem fluorescent-tagged LC3. Autophagy *3*, 452–460.

Krakauer, T. (2019). Inflammasomes, Autophagy, and Cell Death: The Trinity of Innate Host Defense against Intracellular Bacteria. Mediators Inflamm. *2019*, 2471215.

Kuehn, M.J., and Kesty, N.C. (2005). Bacterial outer membrane vesicles and the host–pathogen interaction. Genes Dev. *19*, 2645–2655.

Kulp, A., and Kuehn, M.J. (2010). Biological Functions and Biogenesis of Secreted Bacterial Outer Membrane Vesicles. Annu. Rev. Microbiol. *64*, 163–184.

Lee, C.H., and Tsai, C.M. (1999). Quantification of bacterial lipopolysaccharides by the purpald assay: measuring formaldehyde generated from 2-keto-3-deoxyoctonate and heptose at the inner core by periodate oxidation. Anal. Biochem. *267*, 161–168.

Loos, B., du Toit, A., and Hofmeyr, J.-H.S. (2014). Defining and measuring autophagosome flux—concept and reality. Autophagy *10*, 2087–2096.

Losier, T.T., Akuma, M., McKee-Muir, O.C., LeBlond, N.D., Suk, Y., Alsaadi, R.M., Guo, Z., Reshke, R., Sad, S., Campbell-Valois, F.-X., et al. (2019). AMPK Promotes Xenophagy through Priming of Autophagic Kinases upon Detection of Bacterial Outer Membrane Vesicles. Cell Rep. *26*, 2150-2165.e5.

McPhee, J.B., Small, C.L., Reid-Yu, S.A., Brannon, J.R., Le Moual, H., and Coombes, B.K. (2014). Host Defense Peptide Resistance Contributes to Colonization and Maximal Intestinal Pathology by Crohn's Disease-Associated Adherent-Invasive Escherichia coli. Infect. Immun. *82*, 3383–3393.

Mizushima, N., Yoshimori, T., and Levine, B. (2010). Methods in mammalian autophagy research. Cell *140*, 313–326.

Muñoz-Braceras, S., and Escalante, R. (2016). Analysis of Relevant Parameters for Autophagic Flux Using HeLa Cells Expressing EGFP-LC3. In Proteostasis: Methods and Protocols, R. Matthiesen, ed. (New York, NY: Springer), pp. 313–329.

Murase, K., Martin, P., Porcheron, G., Houle, S., Helloin, E., Pénary, M., Nougayrède, J.-P., Dozois, C.M., Hayashi, T., and Oswald, E. (2016). HlyF Produced by

Extraintestinal Pathogenic Escherichia coli Is a Virulence Factor That Regulates Outer Membrane Vesicle Biogenesis. J. Infect. Dis. *213*, 856–865.

Netea-Maier, R.T., Plantinga, T.S., van de Veerdonk, F.L., Smit, J.W., and Netea, M.G. (2015). Modulation of inflammation by autophagy: Consequences for human disease. Autophagy *12*, 245–260.

de Oliveira, A.L., Rocha, D.A., Finkler, F., de Moraes, L.B., Barbieri, N.L., Pavanelo, D.B., Winkler, C., Grassotti, T.T., de Brito, K.C.T., de Brito, B.G., et al. (2015). Prevalence of ColV Plasmid-Linked Genes and In Vivo Pathogenicity of Avian Strains of Escherichia coli. Foodborne Pathog. Dis. *12*, 679–685.

Peigne, C., Bidet, P., Mahjoub-Messai, F., Plainvert, C., Barbe, V., Médigue, C., Frapy, E., Nassif, X., Denamur, E., Bingen, E., et al. (2009). The Plasmid of Escherichia coli Strain S88 (O45:K1:H7) That Causes Neonatal Meningitis Is Closely Related to Avian Pathogenic E. coli Plasmids and Is Associated with High-Level Bacteremia in a Neonatal Rat Meningitis Model. Infect. Immun. *77*, 2272–2284.

van der Poll, T., van de Veerdonk, F.L., Scicluna, B.P., and Netea, M.G. (2017). The immunopathology of sepsis and potential therapeutic targets. Nat. Rev. Immunol. *17*, 407–420.

Pugsley, H.R. (2017). Quantifying autophagy: Measuring LC3 puncta and autolysosome formation in cells using multispectral imaging flow cytometry. Methods San Diego Calif *112*, 147–156.

Qian, S., Fan, J., Billiar, T.R., and Scott, M.J. (2017). Inflammasome and Autophagy Regulation: A Two-way Street. Mol. Med. *23*, 188–195.

Qiu, P., Liu, Y., and Zhang, J. (2019). Review: the Role and Mechanisms of Macrophage Autophagy in Sepsis. Inflammation *42*, 6–19.

Rolhion, N., Barnich, N., Claret, L., and Darfeuille-Michaud, A. (2005). Strong decrease in invasive ability and outer membrane vesicle release in Crohn's disease-associated adherent-invasive Escherichia coli strain LF82 with the yfgL gene deleted. J. Bacteriol. *187*, 2286–2296.

Rueter, C., and Bielaszewska, M. (2020). Secretion and Delivery of Intestinal Pathogenic Escherichia coli Virulence Factors via Outer Membrane Vesicles. Front. Cell. Infect. Microbiol. *10*.

Saitoh, T., Fujita, N., Jang, M.H., Uematsu, S., Yang, B.-G., Satoh, T., Omori, H., Noda, T., Yamamoto, N., Komatsu, M., et al. (2008). Loss of the autophagy protein Atg16L1 enhances endotoxin-induced IL-1beta production. Nature *456*, 264–268.

Santos, J.C., Dick, M.S., Lagrange, B., Degrandi, D., Pfeffer, K., Yamamoto, M., Meunier, E., Pelczar, P., Henry, T., and Broz, P. (2018). LPS targets host guanylate-binding proteins to the bacterial outer membrane for non-canonical inflammasome activation. EMBO J. e98089.

Sarowska, J., Futoma-Koloch, B., Jama-Kmiecik, A., Frej-Madrzak, M., Ksiazczyk, M., Bugla-Ploskonska, G., and Choroszy-Krol, I. (2019). Virulence factors, prevalence and

potential transmission of extraintestinal pathogenic Escherichia coli isolated from different sources: recent reports. Gut Pathog. *11*, 10.

Schroder, K., Kanneganti, T.-D., Shao, F., and Broz, P. (2018). Mechanisms and Consequences of Inflammasome Activation. J. Mol. Biol. *430*, 131–132.

Schwechheimer, C., and Kuehn, M.J. (2015). Outer-membrane vesicles from Gram-negative bacteria: biogenesis and functions. Nat. Rev. Microbiol. *13*, 605–619.

Soysal, N., Mariani-Kurkdjian, P., Smail, Y., Liguori, S., Gouali, M., Loukiadis, E., Fach, P., Bruyand, M., Blanco, J., Bidet, P., et al. (2016). Enterohemorrhagic Escherichia coli Hybrid Pathotype O80:H2 as a New Therapeutic Challenge. Emerg. Infect. Dis. *22*, 1604–1612.

Vanaja, S.K., Russo, A.J., Behl, B., Banerjee, I., Yankova, M., Deshmukh, S.D., and Rathinam, V.A.K. (2016). Bacterial Outer Membrane Vesicles Mediate Cytosolic Localization of LPS and Caspase-11 Activation. Cell *165*, 1106–1119.

Zhuge, X., Sun, Y., Xue, F., Tang, F., Ren, J., Li, D., Wang, J., Jiang, M., and Dai, J. (2018). A Novel PhoP/PhoQ Regulation Pathway Modulates the Survival of Extraintestinal Pathogenic Escherichia coli in Macrophages. Front. Immunol. *9*, 788.

Figure 1. Increased autophagosomes numbers in epithelial cells treated by OMVs from *E.coli* producing HlyF. (**A**) Images of purified OMVs with equivalent volumes from wild type SP15 (SP15 WT) and from SP15Δ*hlyF* visualized by negative staining transmission electron microscopy (TEM). Scale bar = 100nm. (**B-C**) Images of confocal microscopy of LC3-GFP (green) and DAPI (blue) in LC3-GFP-Hela cells treated 3hr with supernatant from wild type SP15 (SP15 WT) and SP15 *hlyF*- 250µL/mL after ultrafiltration (**B**) or with purified OMV with equivalent protein dosage from wild type SP15 (SP15 WT) 10µg/mL, SP15Δ*hlyF* 10µg/mL and SP15Δ$hlyF_{\text{GST-HlyF}}$ 1µg/mL (**C**). Scale bar = 10µm. (**D**). Images of purified OMV with equivalent protein dosage from BL21 expressing HlyF WT or inactivated (Mut) visualized by negative staining TEM. Scale bar = 100nm. (**E**) Images of confocal microscopy of LC3-GFP (green) and DAPI (blue) in LC3-GFP-Hela cells treated 3hr with OMV BL21 HlyF WT and OMV BL21 HlyF Mut 5µg/mL. Scale bar = 10µm. (**F**) Western blot analysis of LC3 and actin in cell extracts of Hela cells treated 3hr with OMV from BL21 HlyF WT and OMV BL21 HlyF Mut 5µg/mL.

Figure 2. OMVs-induced increase of autophagosomes numbers is dose-dependent and stable. (**A**) Images acquired by ISX of GFP-LC3 HeLa cells treated 3hr with OMV from BL21 HlyF WT 5µg/mL. On the left panel, brightfield channel (BF) images the cells according to their size and morphology, on the right panel, LC3 channel images cells according to their fluorescence in GFP-LC3 in green. Number of LC3 green dots of LC3-GFP per cell is indicated in blue in the dial at the top right of the BF channel. The mask is shown in red on the BF. Bars, 7µm. Images representatives of 4 independent experiments. (**B**) Quantification of (A). Number of LC3 green dots of LC3-GFP per cell counted with the Spot count function is indicated on the vertical axis. Each square represents a cell image acquired by ISX. The graphs show the mean for each condition. ****$p<0.0001$ t test. Graph representative of 4 independent experiments. (**C**) Hela cells were treated with OMV from BL21 HlyF WT 5µg/mL for the indicated time period then LC3 and actin were analyzed by western blot. (**D**) Hela cells were treated with increasing concentrations of OMV from BL21 HlyF WT for 3hrthen LC3 and actin were analyzed by western blot.

Figure 3. Autophagy flux is blocked by OMVs from *E.coli* producing HlyF. (**A**) Schema of the autophagic flux and of the accumulation of different autophagic structures

depending on the autophagic dynamic regulation (adapted from Mizushima et al., 2010). (**B-C**) Hela or LC3-GFP Hela cells were treated with OMVs from BL21 HlyF WT 5µg/mL and/or 50µM chloroquine for 3hr before LC3 and actin western-blot (**B**) and ISX (**C**) analysis. On the left panel, brightfield channel (BF) images, on the right panel, LC3 channel image cells according to their fluorescence in GFP-LC3 in green Bars, 7µm. Images representatives of 3 independent experiments. (**D**) Quantification of (**C**). Number of LC3 green dots of LC3-GFP per cell counted with the Spot count function is indicated on the vertical axis, on a minimum of 3000 cells per condition. Each square represents a cell image acquired by ISX. The graphs show the mean for each condition. Experiment reproduced 3 times independently, ****$p<0.0001$ t test.

Figure 4. Autophagy flux blocked by OMVs at lysosomal fusion step. (**A**) Confocal images of DiFluo Hela cells deprived with HBSS or treated for 3hr with chloroquine or with OMVs from BL21 HlyF WT 5µg/mL. Images of LC3-GFP fluorescence (green), LC3-RFP fluorescence (red), and the overlay with DAPI (blue) which shows co-localization of GFP and RFP fluorescent dyes in yellow. Scale bar = 10µm. 50 cells were analyzed per condition. Representative of 3 independent experiments. (**B**) Images acquired by ISX of DiFluo Hela cells deprived with HBSS or treated for 3hr with chloroquine or with OMVs from BL21 HlyF WT 5µg/mL. On the left panel, brightfield channel (BF), on the medium panel, LC3-GFP channel images cells according to their fluorescence in GFP in green and on the right panel LC3-RFP channel images cells according to their fluorescence in RFP in red. Bars, 7 µm. Images representatives of 3 independent experiments. (**C**) Quantification of BDI (GFP and RFP) by ISX of DiFluo Hela cells deprived with HBSS or treated for 3hr with chloroquine 50µM or with OMVs from BL21 HlyF WT 5µg/mL. Each square represents the ratio of the intensity of RFP and GFP within a cell. The graph shows mean and standard deviations. Representative of 3 independent experiments. ****$p< 0.0001$ t test. (**D**) Confocal images of LC3-GFP (green), LysoTracker Red (red) and DAPI (blue) fluorescence in LC3-GFP Hela cells. The cells were incubated with OMVs from BL21 HlyF WT 5µg/mL for 3hr and LysoTracker Red for 1hr. 100 cells were analyzed per condition. Scale bar = 10µm. Arrows indicates colocalization foci.

Figure 5. OMVs from pathogenic HlyF-expressing *E. coli* induce a stronger activation of the non-canonical inflammasome pathway compared to OMVs from *E. coli* expressing a non-functional HlyF protein. (**A**) IL-1β secretion from unprimed WT, Casp1$^{-/-}$ /Casp11$^{-/-}$ BMDMs infected for 24 h with OMV HlyF WT and OMV HlyF Mut 10µg/mL. (**B**) Western-blot analysis of cleaved caspase-1 (p20), and Gasdermin-D in cell supernatants (sup) and of pro-caspase-1, Gasdermin-D and GAPDH (loading control) in cell extracts of unprimed WT or Casp11$^{-/-}$ BMDMs (Cells) treated for 8h with 10µg/mL OMVs BL21 HlyF Mut, OMVs BL21 HlyF WT, transfected LPS from OMVs BL21 HlyF Mut or from OMVs BL21 HlyF WT (1µg/mL using FuGENE HD, Promega).

Figure 1

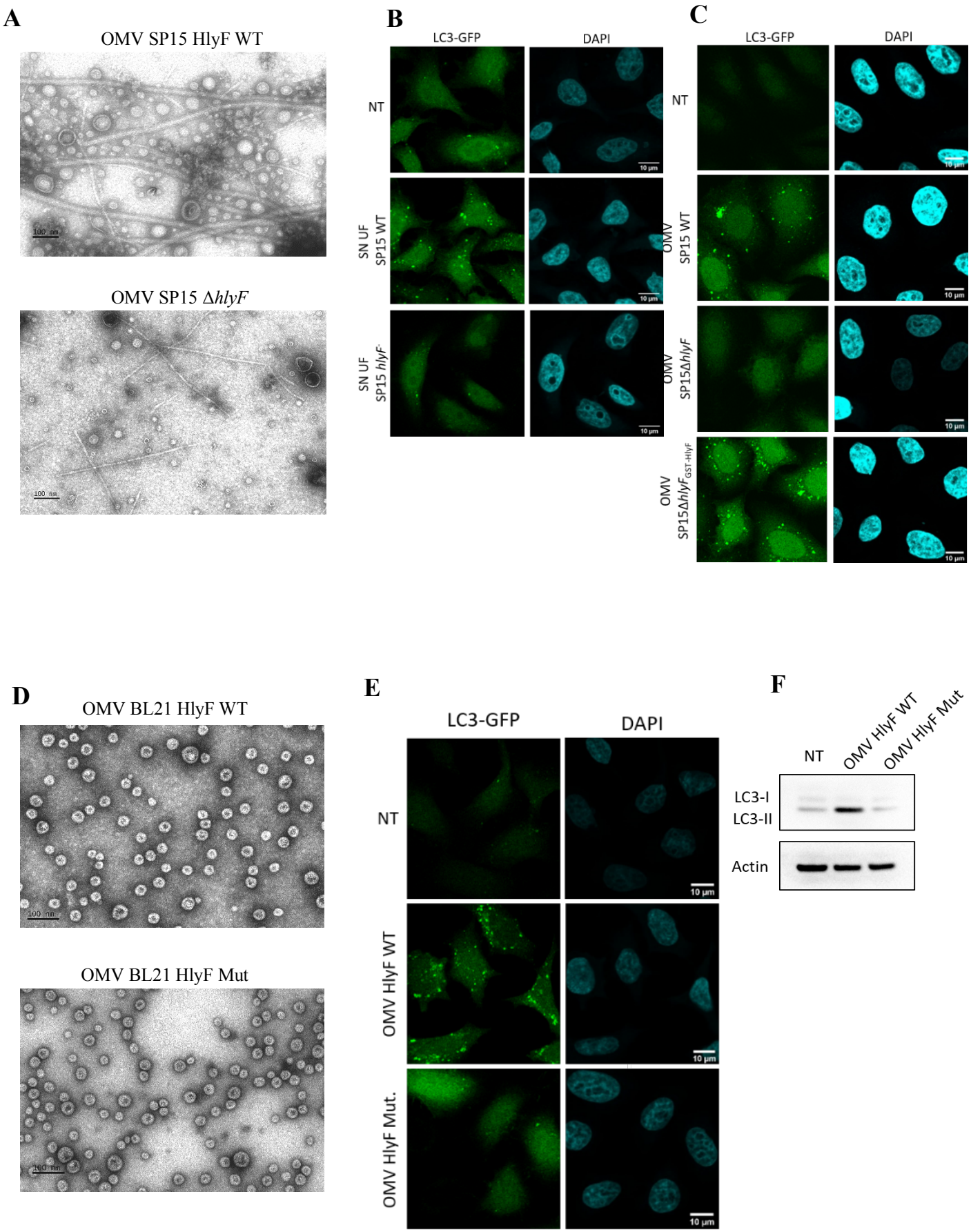
A
OMV SP15 HlyF WT
OMV SP15 ΔhlyF
B
LC3-GFP
DAPI
NT
SN UF SP15 WT
SN UF SP15 hlyF-
C
LC3-GFP
DAPI
NT
OMV SP15 WT
OMV SP15ΔhlyF
OMV SP15ΔhlyF GST-HlyF
D
OMV BL21 HlyF WT
OMV BL21 HlyF Mut
E
LC3-GFP
DAPI
NT
OMV HlyF WT
OMV HlyF Mut.
F
NT
OMV HlyF WT
OMV HlyF Mut
LC3-I
LC3-II
Actin

Figure 2

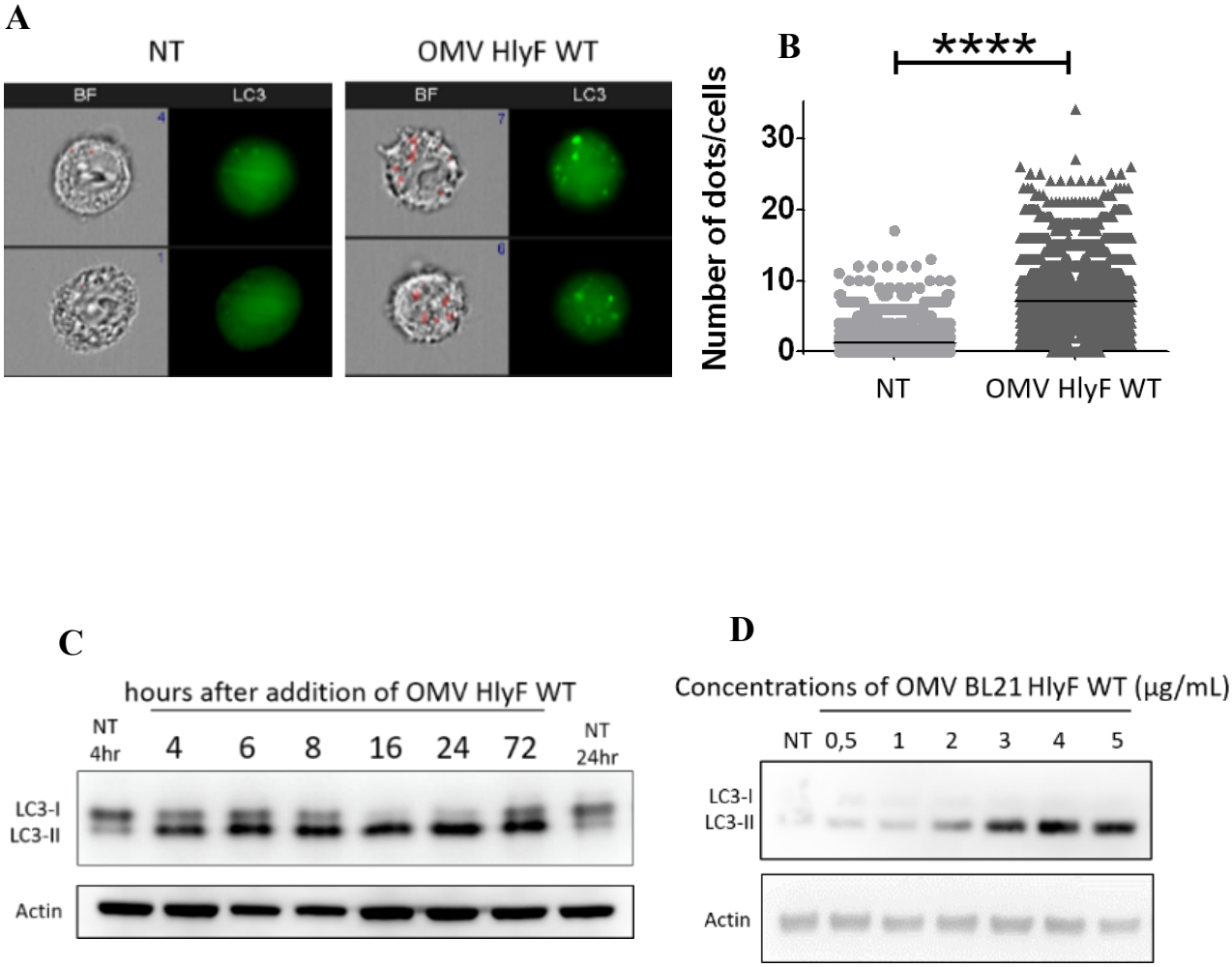
A
NT
OMV HlyF WT
BF
LC3
BF
LC3
B
****
Number of dots/cells
30
20
10
0
NT
OMV HlyF WT
C
hours after addition of OMV HlyF WT
NT 4hr
4
6
8
16
24
72
NT 24hr
LC3-I
LC3-II
Actin
D
Concentrations of OMV BL21 HlyF WT (µg/mL)
NT
0,5
1
2
3
4
5
LC3-I
LC3-II
Actin

Figure 3

A

	Phagophore	Autophagosome	Autolysosome
Autophagic flux	+	+	+
Autophagic flux blocked	+	++	-
Autophagic flux increased	++	++	++

B

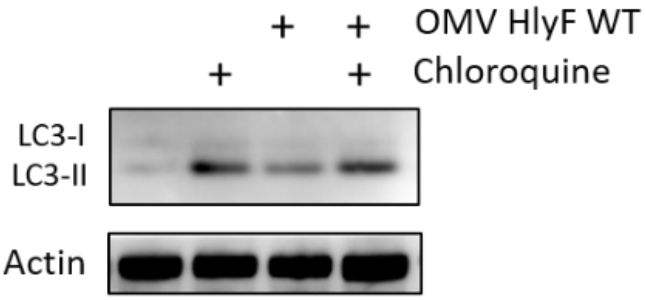

C

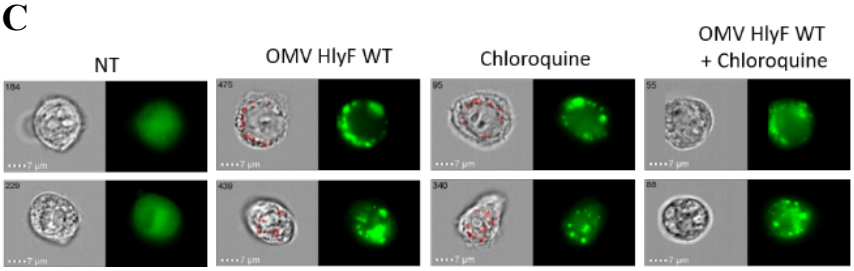

D

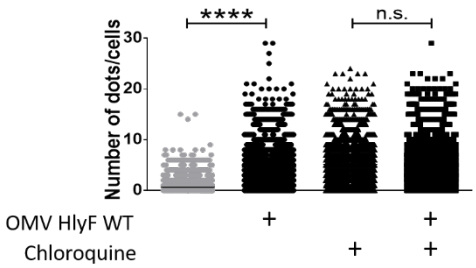

Figure 4

A

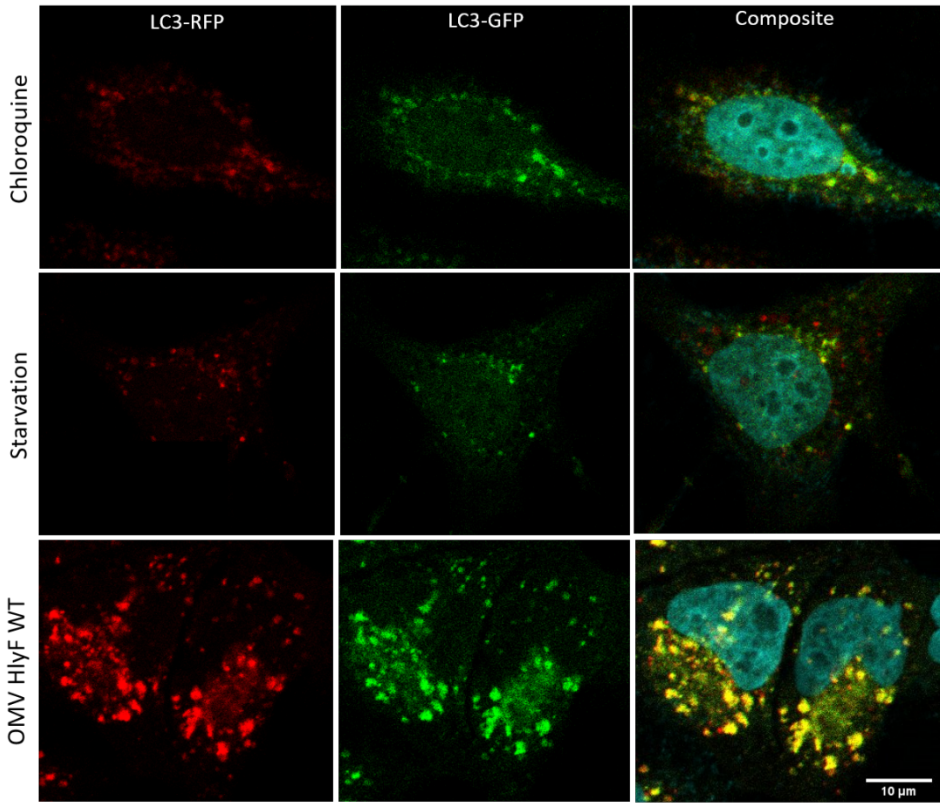

B

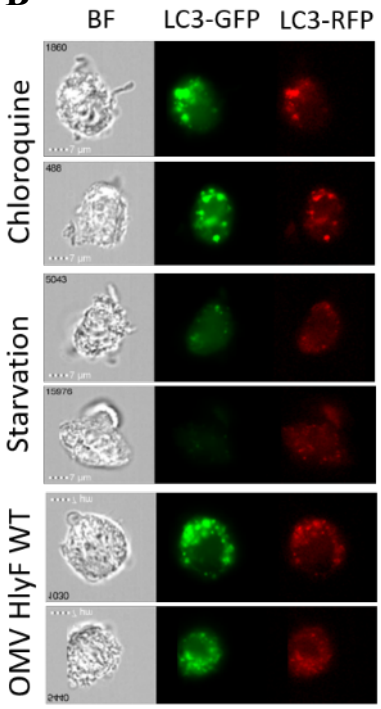

C

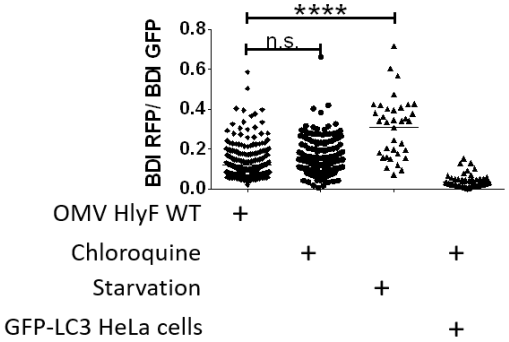

D

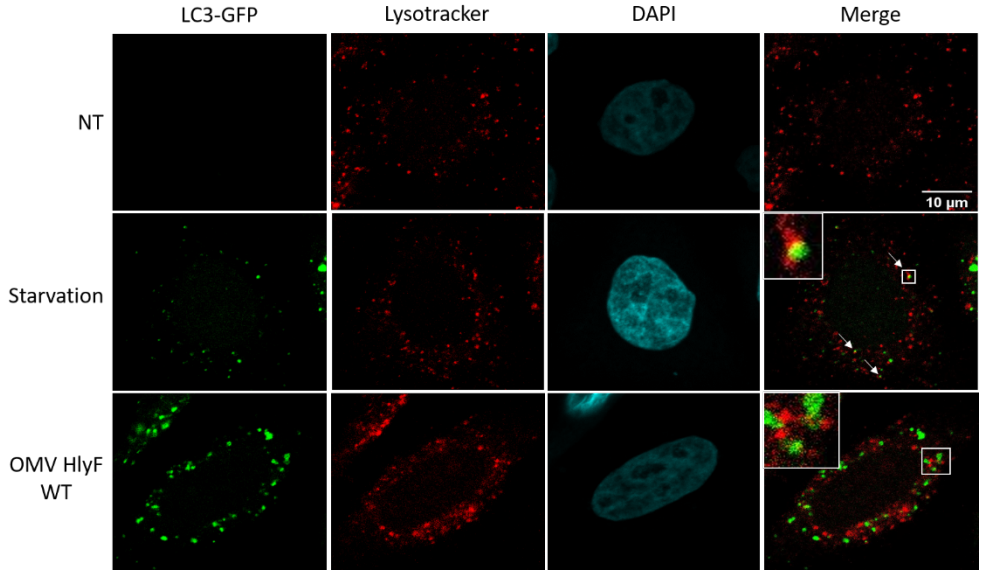

Figure 5

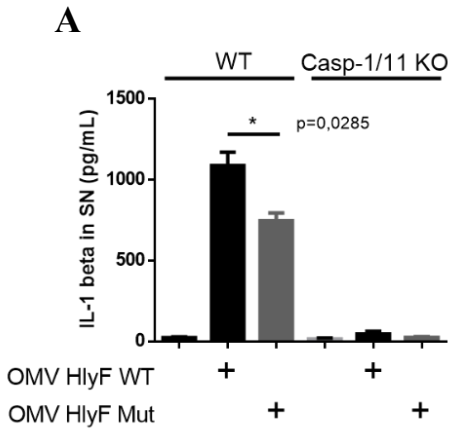
A
WT
Casp-1/11 KO
IL-1 beta in SN (pg/mL)
1500
1000
500
0
*
p=0,0285
OMV HlyF WT
OMV HlyF Mut
+
+
+
+

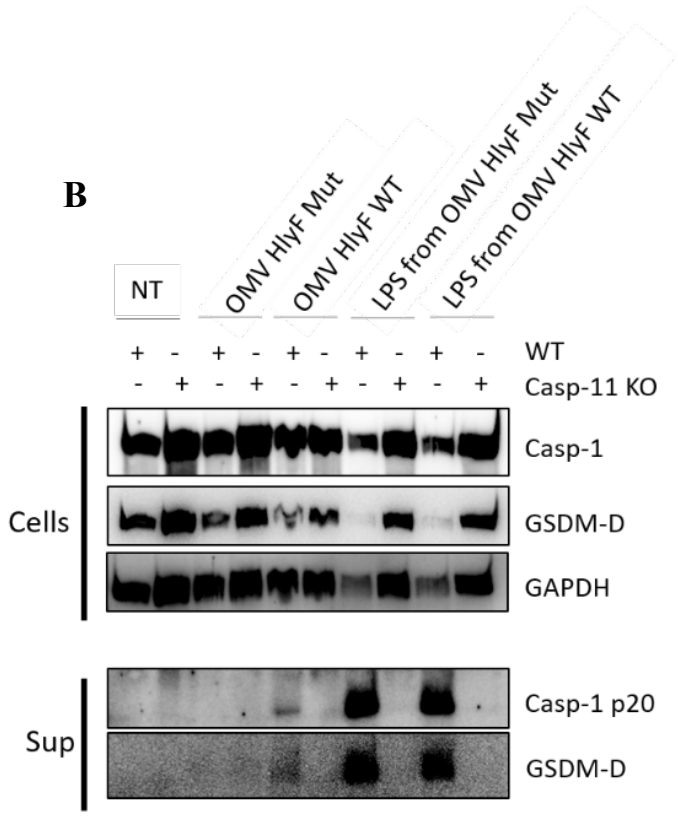
B
NT
OMV HlyF Mut
OMV HlyF WT
LPS from OMV HlyF Mut
LPS from OMV HlyF WT
WT
Casp-11 KO
Cells
Casp-1
GSDM-D
GAPDH
Sup
Casp-1 p20
GSDM-D